Band-structure-corrected local density approximation study of semiconductor quantum dots and wires

Jingbo Li and Lin-Wang Wang*
Computational Research Division, Lawrence Berkeley National Laboratory, Berkeley, California 94720, USA
(Received 2 May 2005; revised manuscript received 19 July 2005; published 16 September 2005)

This paper presents results of *ab initio* accuracy thousand atom calculations of colloidal quantum dots and wires using the charge patching method. We have used density functional theory under local density approximation (LDA), and we have corrected the LDA bulk band structures by modifying the nonlocal pseudopotentials, so that their effective masses agree with experimental values. We have systematically studied the electronic states of group III-V (GaAs, InAs, InP, GaN, AlN, and InN) and group II-VI (CdSe, CdS, CdTe, ZnSe, ZnS, ZnTe, and ZnO) systems. We have also calculated the electron-hole Coulomb interactions in these systems. We report the exciton energies as functions of the quantum dot sizes and quantum wire diameters for all the above materials. We found generally good agreements between our calculated results and experimental measurements. For CdSe and InP, the currently calculated results agree well with the previously calculated results using semiempirical pseudopotentials. The ratios of band-gap-increases between quantum wires and dots are material-dependent, but a majority of them are close to 0.586, as predicted by the simple effective-mass model. Finally, the size dependence of $1S_e$-$1P_e$ transition energies of CdSe quantum dots agrees well with the experiment. Our results can be used as benchmarks for future experiments and calculations.

DOI: 10.1103/PhysRevB.72.125325 PACS number(s): 73.22.−f, 71.15.Mb, 79.60.Jv

I. INTRODUCTION

During the past 20 years, various semiconductor nanocrystals have been synthesized and it has been found that their electrical and optical properties are dramatically different from their bulk counterparts.[1–13] A typical semiconductor nanocrystal with 1–10 nm diameter consists of about 100–10000 atoms. These small colloidal nanocrystals as promising advanced functional materials can be found in many different applications, ranging from lasers,[14–16] solar cells,[17] to single-electron transistors.[18] One example of these nanocrystal applications is to incorporate them into biological systems.[19–22] CdSe quantum dots (QDs) permit *in vivo* cancer cell targeting and imaging in living mice.[23] Many of these applications are related to the size-dependence of the nanocrystal optical properties. In a semiconductor, the optical properties are related to the edge transitions of the electronic band gaps. Thus, studying the size dependence of the electron band gap and the related exciton energy is one of the most important topics in semiconductor nanocrystal research.

Following different manufacturing processes, the nanocrystals can be grown in different matrices, such as polymers; cavities of zeoliths, glasses, and solutions; and organic molecules or biomolecules. In many cases, the surface dangling bond electronic states have been removed by the matrices. In these cases, their electronic and optical properties become the intrinsic features of the nanosystem, independent of the enclosure matrices and surface passivations. Thus, one of the main tasks in QD research is to study the dependencies of these intrinsic properties to the sizes of the QDs. Besides the change in size, change in shape also leads to different electronic states and energy band gaps in nanocrystals.[24] With rapid developments in chemical synthesis, the control of nanocrystal size, shape, and dimensionality[25–31] have become possible. The shape effects can be very useful in light-emission applications. For example, a recent experiment[32,33] has found that the lack of a large overlap between absorption and emission spectra in CdSe quantum rods (QRs) can improve the efficiency of light-emitting diodes (LEDs) due to the reduction in reabsorption. Spherical-shaped QDs, which have quantum confinements in all three dimensions, have been studied extensively. But the study in QRs and quantum wires (QWs) are just beginning. As the length of a QR increases, it becomes a QW, which is confined in two dimensions. In this work, we will focus on the electronic structures of semiconductor QDs and QWs.

There have been many theoretical works about the electronic structures of QDs and QWs. Several theoretical approaches have been used in these studies. One is the continuum $k\cdot p$ effective-mass method. This is the most widely used method,[34–43] borrowed from bulk quantum well and exciton studies. However, this method has several shortcomings, especially for small colloidal nanocrystals. For example, the small sizes of the QD might be beyond the valid range of the continuum $k\cdot p$ model in reciprocal space, and there is an ambiguity for the $k\cdot p$ boundary condition. The second widely used method in nanostructure calculation is the tight-binding model.[44–49] The tight-binding model can be used to study thousand-atom systems easily, and it has been proved to be highly successful. However, it is sometimes difficult to fit the conduction band band structure. In addition, there is no information about the atomic features of the wave functions. The third method for nanocrystal study is the empirical pseudopotential method (EPM). The original EPM was developed in the 1960s to describe the bulk band structures of semiconductors; it uses a sum of non-self-consistent screened pseudopotentials to represent the total potential of a system, and it also uses a variationally flexible plane wave basis to describe the electron wave function. Recently, EPM has been adapted to calculate nanocrystals. It has also been

improved by (1) fitting it to the *ab initio* bulk potentials; (2) adding local environment-dependent prefactors to describe the deformation potentials; and (3) rescaling the kinetic energy operator to mimic the effects of nonlocal potentials. These improvements have allowed us to describe the electronic structure of nanosystems accurately.[50–57] Despite the success of the EPM method, there are still problems that need to be resolved. One problem of the EPM calculation for free-standing colloidal systems is the surface passivation. While it is easy to fit a bulk EPM, it is often difficult to find the corresponding surface passivation potentials. As a result, the EPM method and its improved version, semiempirical pseudopotential method (SEPM), have been limited to a few semiconductor materials (e.g., Si, Ge, InAs, InP, CdSe) for colloidal nanocrystal studies. The fourth method to calculate the electronic structure of a nanocrystal is to use *ab initio* methods,[58–63] such as the density functional theory (DFT). This method is more reliable than the EPM approach and can be used for almost any materials. One disadvantage of this method is the large computational time required for thousand atom nanostructure calculations. Besides, if the DFT method with the local density approximation (LDA) is used, there is often a band gap problem that needs to be addressed.

One recent development in nanoscience and technology is the synthesis of myriad types of nanocrystals by various chemical methods. It may seem that nanosized QDs and QWs can be synthesized for almost any given binary semiconductor compounds, for both group II-VI and group III-V. However, the EPM method that we have been using is limited to a few semiconductor materials due to the difficulty in getting good surface passivations. In the EPM approach, without a good surface passivation, the interior band edge states cannot be calculated. In this paper, we will use the newly developed charge patching method to calculate QDs and QWs for various semiconductor materials. This is essentially an *ab initio* DFT method, but without the computational cost of a direct DFT calculation. We will use partially charged pseudohydrogen atoms to passivate the surface. As will be explained in Sec. II, this represents a simple but ideal passivation that removes the surface dangling bond states. The charge patching method reproduces the LDA charge densities without doing direct LDA calculations for the whole system. We have also modified the LDA band structure, so the effective mass (which is critical to the quantum confinement effect) is corrected when compared to experimental values. Combining these methods, we have a complete approach to calculate the electronic structures and optical properties of QDs and QWs for any given semiconductor materials. The purpose of this paper is to present the results of such calculations, and to compare these results with known experimental measurements. For systems there are still no good experimental measurements, our results can serve as predictions to guide future experiments. Our results can also be used as benchmarks for future theoretical works, since for many of these systems, this is the first time the *ab initio* results have been calculated.

We would like to compare with a few types of experimental measurements in this paper.

(1) *Photoluminescence (PL) measurements of the quantum confinement effects*. The most direct way to detect the quantum confinement effect is to measure the photoluminescence of the nanocrystals.[62–65] The PL measures the lowest exciton energy of the system. However, the exciton energy includes the single particle band gap energy and the electron-hole Coulomb interaction energy. Thus, in order to compare with the experimental measurements, we also need to calculate the Coulomb interaction energies, along with single particle eigenenergies.

(2) *High energy excitation in quantum dots or rods*. Recently, there have been many experiments to investigate and assign the excited states of QDs or QRs (Refs. 34 and 66–69) by the size-selective technique of photoluminescence excitation (PLE). The energy spacings of a series of the higher excited states can vary with the size of QDs. This has inspired many theoretical investigations into this problem.[34,70–73] In this work, we will calculate the PLE of CdS QDs.

(3) *Ratio of confinement-energies between quantum wires and dots*. Recently, high-quality semiconductor QWs have been fabricated by solution-liquid-solid approaches.[12,64,65] The diameters of the quantum wires synthesized in this way are small enough to show strong quantum confinement effects just as in colloidal quantum dots. This provides an opportunity to study the dimensionality dependence of the quantum confinement effects. According to a simple effective-mass approximation model,[73–75] the band gap increases of QDs and QWs from the bulk value are

$$\Delta E_g = \frac{2\hbar^2\zeta^2}{m^* D^2},$$

where

$$\frac{1}{m^*} = \frac{1}{m_e^*} + \frac{1}{m_h^*}$$

m_e^* and m_h^* are electron's and hole's effective masses, respectively, and D is the QD and QW diameter. For spherical QDs, $\zeta = \pi$ is the zero point of the spherical Bessel function, while for cylindrical QWs, $\zeta = 2.4048$ is the zero point of the cylindrical Bessel function. Thus the ratio of band gap increases between the QWs and QDs with the same size D should be $\Delta E_g^{\text{wire}} / \Delta E_g^{\text{dot}} = 0.586$. The interesting question is, How close are our results to this ratio compared to the simple effective mass result?

(4) *Conduction band S and P state splitting*. Besides the PLE experiment, which can be used to measure the high excited states, the conduction band intraband splitting can be measured more directly using *n*-type doping and the corresponding infrared absorption.[76–78] Compared with PLE, which measures the exciton energies, the intraband transition measurement is more direct, and involves only conduction band states. We will report the results of $1S_e$-$1P_e$ transition energy for CdSe QDs.

II. CALCULATION METHOD

A. LDA calculations for bulk materials

We first calculate the band structures of bulk materials via a self-consistent plane-wave pseudopotential (PWP) method,

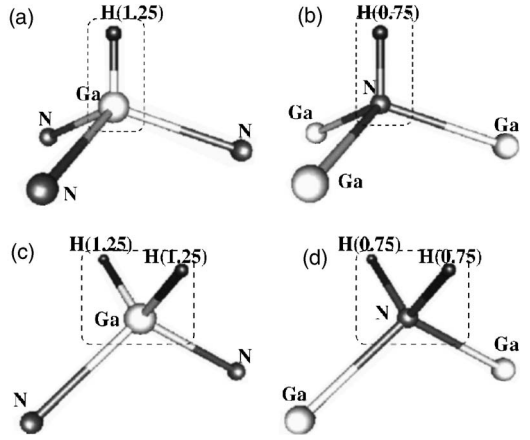

FIG. 1. Schematic configuration for Ga-terminated and N-terminated surface. Dangling bonds passivated by H contain 1.25 and 0.75 electrons on the Ga-terminated and As-terminated ideal surface, respectively. The surface charge-density motifs are generated for the group of atoms inside the dashed line square box. (a) Ga-terminated surface passivated by one H atom. (b) N-terminated surface passivated by one H atom. (c) Ga-terminated surface passivated by two H atoms. (d) N-terminated surface passivated by two H atoms.

based on LDA of the DFT. The single-particle wave function ψ_i and its eigenenergy ε_i are solved by Schrödinger's (Kohn-Sham) equation,

$$\left[-\tfrac{1}{2}\nabla^2 + V^{\mathrm{ps}}_{\mathrm{nonlocal}}(\mathbf{r}) + V_{\mathrm{LDA}}(\mathbf{r})\right]\psi_i = \varepsilon_i\psi_i, \qquad (1)$$

where $V^{\mathrm{ps}}_{\mathrm{nonlocal}}(\mathbf{r})$ is the nonlocal part of the ionic pseudopotential, which is angular momentum dependent. $V_{\mathrm{LDA}}(\mathbf{r}) = V^{\mathrm{ps}}_{\mathrm{local}}(\mathbf{r}) + V_{\mathrm{HXC}}(\mathbf{r})$ contains the local ionic pseudopotential $V^{\mathrm{ps}}_{\mathrm{local}}(\mathbf{r})$ and the electron Coulomb and LDA exchange correlation potential $V_{\mathrm{HXC}}(\mathbf{r})$. Throughout all of our calculations, we have used the norm-conserving pseudopotentials. We have included the *d* electron in the valence electrons for Zn atoms, but only kept *s* and *p* electrons for other elements. We have used a plane wave cutoff energy of 25–35 Ryd for most systems, except for system containing Zn or the first row elements N and O, where a 65 Ryd cutoff is used. We have used the PEtot (Ref. 79) plane wave pseudopotential package for our calculations. We have ignored the spin-orbit coupling for the valence bands.

B. Surface passivations

The surface of an unpassivated nanocrystal consists of dangling bonds, which will introduce band gap states. The purpose of a good passivation is to remove these band gap states. One way to do so is to pair the unbonded dangling bond electron with other electrons. If a surface atom has m valence electrons, this atom will provide $m/4$ electrons to each of its four bonds in a tetrahedral crystal. To pair these $m/4$ electrons in each dangling bond, a passivating agent should provide $(8-m)/4$ additional electrons. To keep the system locally neutral, there must be a positive $(8-m)/4$ nuclear charge nearby. Thus, the simplest passivation agent can be a hydrogenlike atom with $(8-m)/4$ electrons and a nuclear charge $Z=(8-m)/4$. For IV-IV group materials like Si, this means $Z=1$ (hydrogen atoms). For III-V and II-VI systems, the resulting atoms have a noninteger Z, thus a pseudohydrogen atom. These artificial pseudohydrogen atoms do describe the essence of a good passivation agent, and thus can serve as simplified models for the real passivation situations.

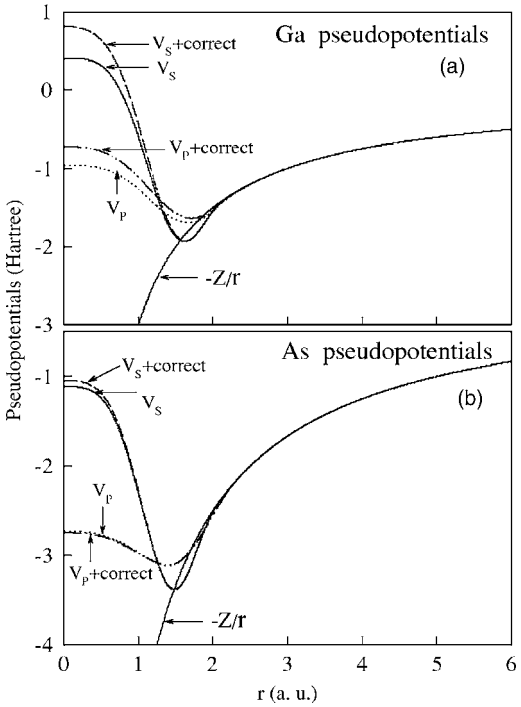

FIG. 2. Pseudopotentials of (a) Ga and (b) As atoms in real space. The nonlocal pseudopotentials are angular momentum dependent. V_s and V_p are the *s* and *p* states of the valence wave functions. The modified pseudopotentials are V_s+correct and V_p +correct, respectively. Z is the pseudo core charge.

This pseudohydrogen model has been used successfully in our previous studies.[63] Here, we will use it to passivate all of our systems. Note, we have $Z=1, 0.75, 0.5, 1.25, 1.5$ for IV, V, VI, III, and II row atoms, respectively. A half bulk bond length is used as the pseudohydrogen atom-surface atom bond length for all the systems. All the band gap states have

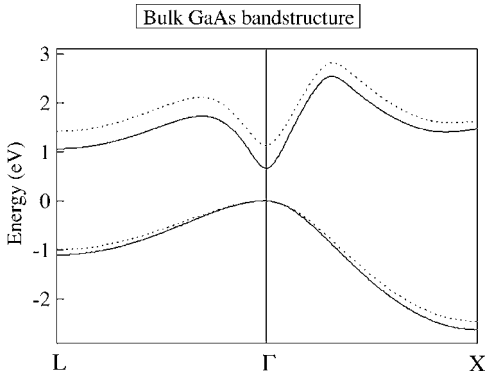

FIG. 3. Band structures of bulk GaAs of LDA self-consistent calculation (solid curves) and of the modified nonlocal pseudopotentials (dotted curves).

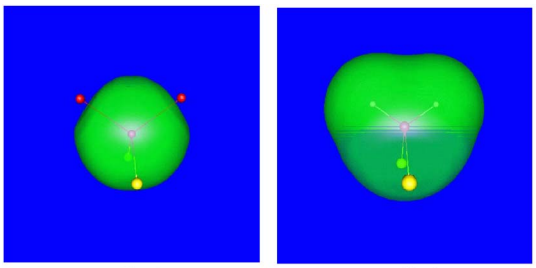

Charge motif of a Ga atom bounded to 2 N (upper) and 2 P (lower) atoms.

Charge motif of a GaH2 group bounded to 2 P atoms

FIG. 4. (Color online) The charge motifs used to generate the charge densities of GaNP systems and GaPH quantum dots. One charge density isosurface is plotted.

been removed, and because of that, our interior nanostructure electron states do not depend sensitively on the details of the surface passivations. One example of the pseudohydrogen passivation for the GaN system is depicted in Fig. 1, where $Z=1.25$ for Ga atom passivations, and $Z=0.75$ for N atom passivations.

C. Correcting the bulk effective masses

One problem of the LDA calculation for the electronic band structure is the severe underestimation of the electron band gap. Related to this, and more significant for our purpose, is the underestimation of the electron effective mass. For example, for GaAs, we obtain $E_g=0.656$ eV and $m_e^*=0.04$ under LDA calculation, both of which are much smaller than the experimental results of $E_g=1.633$ eV and $m_e^*=0.067$, respectively. To describe the quantum confinement effects accurately, we have to correct the shape of the bulk band structure (which is in part indicated by the effective mass). Here, we have modified the nonlocal pseudopotentials of the cations and anions to correct the band structures. Unfortunately, the band gap and the effective mass cannot be corrected simultaneously using this simple potential modification. If the band gap is corrected, the effective mass will be too large. For our purposes, it is more important to correct the band structure shape (e.g., the effective mass), while the absolute band gap error can be corrected by uni-

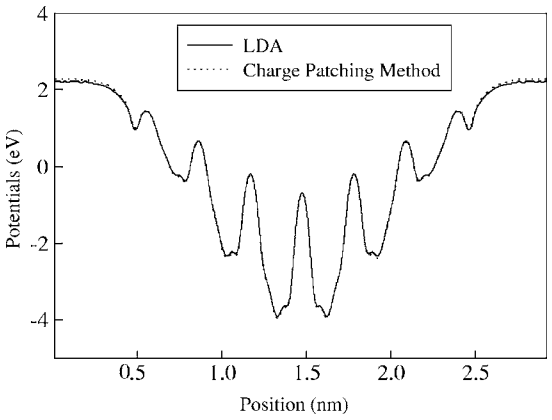

FIG. 5. Planar averaged atomic potentials of CdSe QDs with zinc blende structure. The diameter of QDs is 1.99 nm. The horizontal position axis is along the (100) direction. Potentials from self-consistent LDA calculation and charge patching method are shown by the solid curve and dotted curve, respectively.

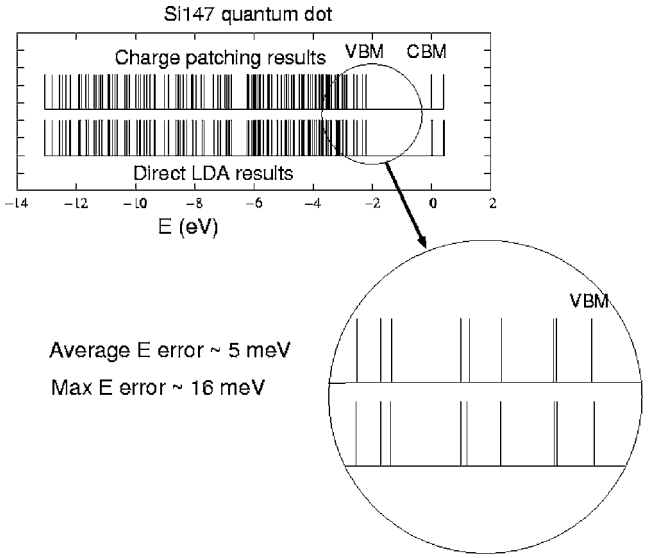

FIG. 6. The single particle eigen energies of a 149 Si atom quantum dot, comparison between the charge patching results, and the direct self-consistent LDA results. Each verticle bar is an eigenenergy.

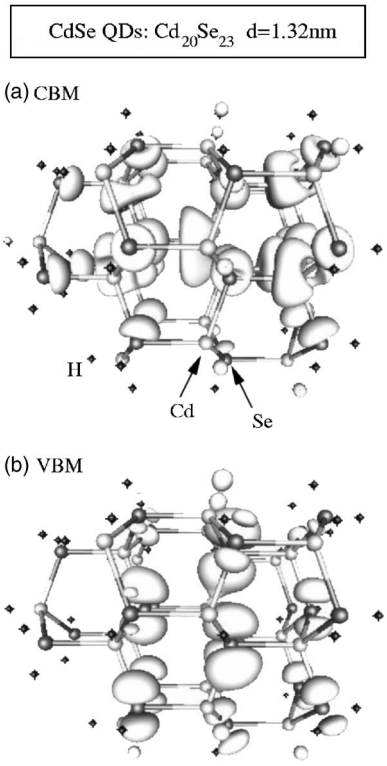

FIG. 7. Wave function isosurfaces of CdSe QDs with 1.32 nm diameter for (a) CBM and (b) VBM states. The bonding geometry of CdSe QDs is a wurtzite structure. Isosurfaces are drawn at 20% of maximum. The small isolated black spheres are the surface passivation pseudo-H atoms.

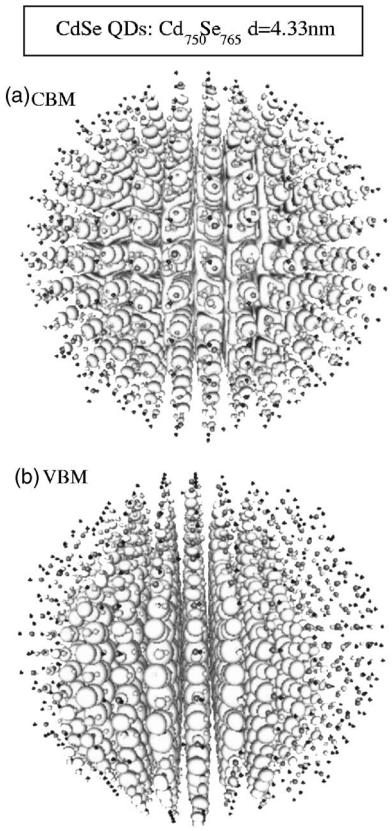

FIG. 8. Same as Fig. 7, but the diameter of the QDs is 4.33 nm.

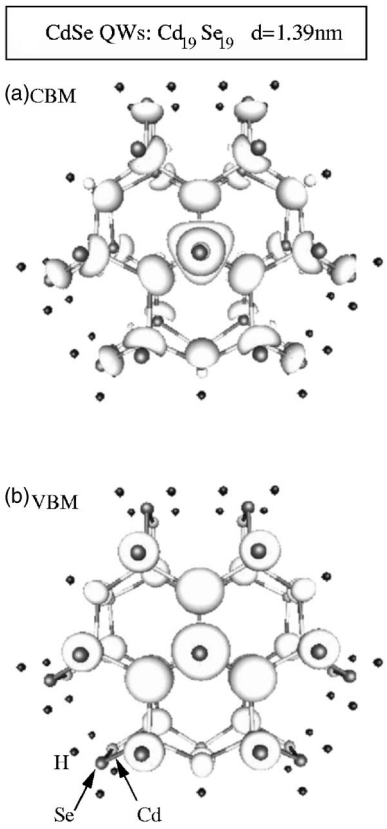

FIG. 9. Same as Fig. 7, but for CdSe QWs with 1.39 nm diameter. We are looking down the QW in the wurtzite (0001) direction.

formly shifting the results for all the QDs and QWs. We have added $\beta \sin(r\pi/r_c)/r$ (zero outside r_c) to the s, p, and d nonlocal pseudopotentials, with r_c fixed at $0.8 \sim 1.2$ Å, and where β is a fitting parameter. We have fitted the effective masses, plus the values of $X_{1c}-\Gamma_{1c}$, $X_{3c}-\Gamma_{1c}$, and $L_{1c}-\Gamma_{1c}$ energies, while the valence band maxima (VBM) are kept at their original LDA values. The modifications of the nonlocal pseudopotentials are relatively small, as shown in Fig. 2, thus many features of the original LDA results (e.g., the deformation potentials) are kept intact. The modified band structure of the bulk GaAs is shown in Fig. 3. The fitting procedure is simple and straightforward. In practice, this is significantly different from the EPM where different fittings can yield dramatically different potentials. For the surface pseudohydrogen atoms, no modification is needed to keep the original good passivations. Note that both in the fitting and in the following large-system calculations, the original pseudopotentials are used in the self-consistent LDA calculations for the charge densities, and the modified nonlocal pseudopotentials are used only in a post process to calculate the electronic structures of the systems.

D. Charge patching method

For nanostructures over several hundred atoms, the direct LDA calculation becomes very expensive. To solve this problem, we have used our newly developed charge patching method. In this method, it is assumed that the charge density at a given point depends only on the local atomic environment around that point. As a result, we have generated charge density motifs for different atoms from small prototype LDA calculations to represent different local atomic environments. These charge motifs can be reassembled to generate the charge density of a large nanosystem without an explicit direct LDA calculation of that system. The details of this method have been published elsewhere.[80] Here, we only give a brief description.

A charge density motif is calculated as

$$m_{I_\alpha}(\mathbf{r}-\mathbf{R}_\alpha) = \rho_{\mathrm{LDA}}(\mathbf{r}) \frac{w_\alpha(|\mathbf{r}-\mathbf{R}_\alpha|)}{\sum_{\mathbf{R}_{\alpha'}} w_{\alpha'}(|\mathbf{r}-\mathbf{R}_{\alpha'}|)}, \qquad (2)$$

where $\mathbf{R}_\alpha$ is an atomic site of atom type α; $m_{I_\alpha}(\mathbf{r}-\mathbf{R}_\alpha)$ is the charge density motif that belongs to this atomic site; and $\rho_{\mathrm{LDA}}(\mathbf{r})$ is the self-consistently calculated charge density of a prototype system. We have used the atomic charge density of the atom α multiplied by an exponential decay function as $w_\alpha(r)$ in Eq. (2). The calculated localized $m_{I_\alpha}(\mathbf{r}-\mathbf{R}_\alpha)$ is stored in a numerical array. We have used a subscript I_α in m_{I_α} to denote the atomic bonding environment of the atom α at $\mathbf{R}_\alpha$. This atomic bonding environment can be defined as the nearest neighbore atomic types of atom α.

To reconstruct the charge density of a given system, the charge motifs for all the atoms are placed together as

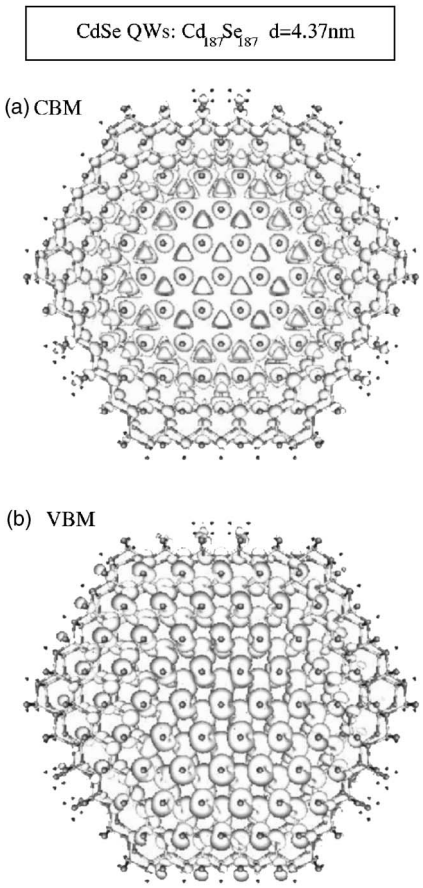

FIG. 10. Same as Fig. 9, but for CdSe QWs with 4.37 nm diameter.

$$\rho_{\text{patch}}(\mathbf{r}) = \sum_{\mathbf{R}_\alpha} m_{I_\alpha}(\mathbf{r} - \mathbf{R}_\alpha). \tag{3}$$

Here, the atomic bonding environment I_α should be the same as in Eq. (2).

After $\rho_{\text{patch}}(\mathbf{r})$ is obtained, the LDA formula can be used to generate the total potential $V_{\text{LDA}}(r)$ in Eq. (1), and the modified nonlocal potential described in Sec. II C can be used to construct the Hamiltonian of a given nanosystem. After these, the linear scaling folded spectrum method (FSM) (Ref. 50) is used to solve the band edge states of a thousand-atom nanostructure.

In Fig. 4, we show the charge motifs used to construct GaNP quantum dots. Although we discuss only binary compounds throughout the rest of this paper, the charge patching method can also be used to calculate ternary semiconductor systems. In Fig. 5, we show the LDA local potential $V_{\text{LDA}}(r)$ in a small CdSe quantum dot generated by the charge patching method and a direct LDA calculation. As we can see, the difference is extremely small. In Fig. 6, we show single-particle eigen energies of a small Si quantum dot, which were calculated using the charge patching method and the direct LDA method. The average eigen energy error is only about 5 meV. From all these tests, we see that the charge patching method is accurate enough to reproduce the *ab initio* LDA electronic structures for thousand-atom systems.

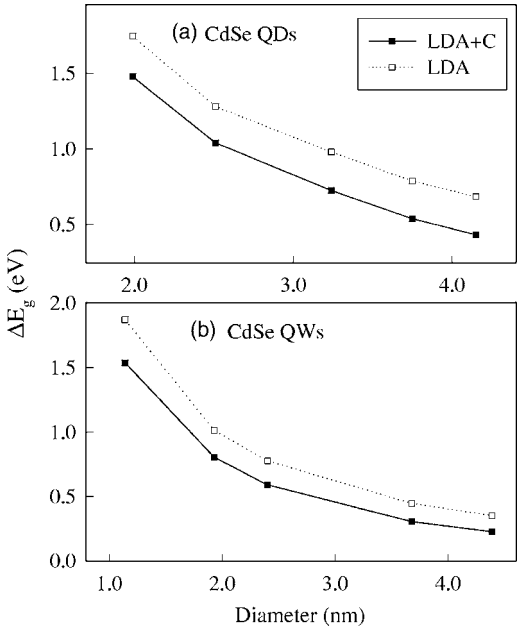

FIG. 11. Comparison of quantum confinement energies by present "LDA+C" calculations (bulk effective-mass is corrected to experiment) and previous "LDA" calculation (no correction on LDA band structure) in CdSe QDs and QWs. The bond geometry of QDs and QWs is zinc blende structure. No Coulomb energy is considered in this figure.

With the modification on the nonlocal pseudopotentials to correct the LDA band structure, this approach can be used to calculate accurately the electronic structures of thousand-atom nanocrystals.

E. Screened electron-hole Coulomb interactions

In nanoscale QDs, the electrons and holes are confined in a small physical space, leading to strong electron-hole Coulomb interactions. To calculate the exciton energy or optical absorption spectrum based on the single-particle states of QDs, a simple approximation is to include the electron-hole

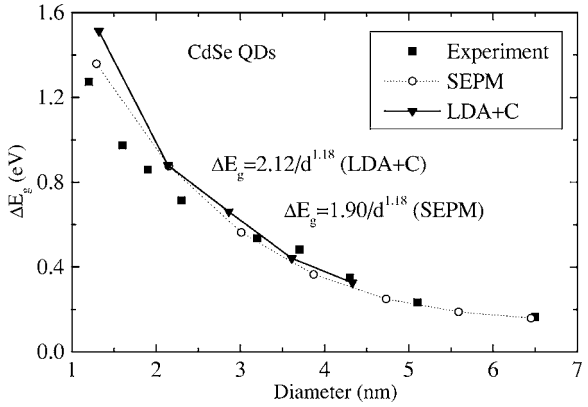

FIG. 12. Comparison of the exciton energy shift (from its bulk value) of CdSe QDs between experiment, "LDA+C" (present work), and SEPM calculations. Coulomb energies are considered in this calculation. Experimental data is from Ref. 5.

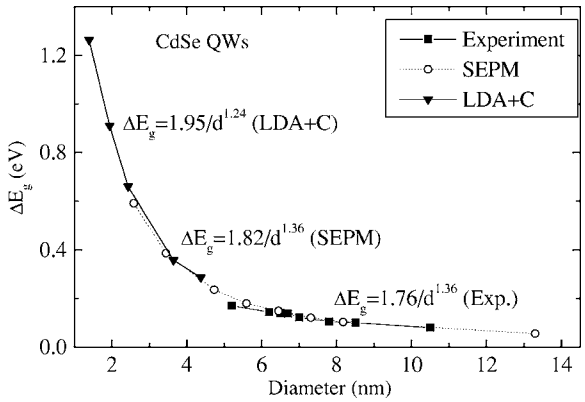

FIG. 13. Comparison of the quantum confinement energy gap of CdSe QWs between experiment, "LDA+C" (present work), and SEPM calculations. Experimental data are from Ref. 65.

Coulomb interaction energy on top of the single-particle band gap. In doing so, we have ignored the electron-hole exchange interaction and possible correlation effects. However, in the strong confinement regime (which is true for most colloidal nanosystems), these effects are very small. Under the above approximation, the exciton energy E_{ex} can be expressed as

$$E_{\mathrm{ex}} = \varepsilon_j - \varepsilon_i - E_{ij}^{C}. \tag{4}$$

Here, ε_i and ε_j are the single-particle valence state and conduction state eigen energies respectively, and E_{ij}^{C} is the electron-hole Coulomb energy calculated as

$$E_{ij}^{C} = \int\int \frac{|\psi_j(\mathbf{r}_1)^2||\psi_i(\mathbf{r}_2)^2|}{\epsilon(\mathbf{r}_1-\mathbf{r}_2)|\mathbf{r}_1-\mathbf{r}_2|} d\mathbf{r}_1 d\mathbf{r}_2, \tag{5}$$

where $\psi_j(\mathbf{r}_1)$ and $\psi_i(\mathbf{r}_2)$ are the calculated electron and hole wave functions, and $\epsilon(\mathbf{r}_1-\mathbf{r}_2)$ is a distance dependent screening dielectric function. We have followed our previous work, using a model dielectric function $\epsilon(\mathbf{r}_1-\mathbf{r}_2)$. More specifically, in the Fourier space, we have first separated the ionic contribution from the electron contribution as $\epsilon^{-1}(k) = \epsilon_{\mathrm{el}}^{-1}(k) + \Delta\epsilon_{\mathrm{ion}}^{-1}(k)$. Then, by using the Thomas-Fermi model of Resta, these two terms have the analytical forms of

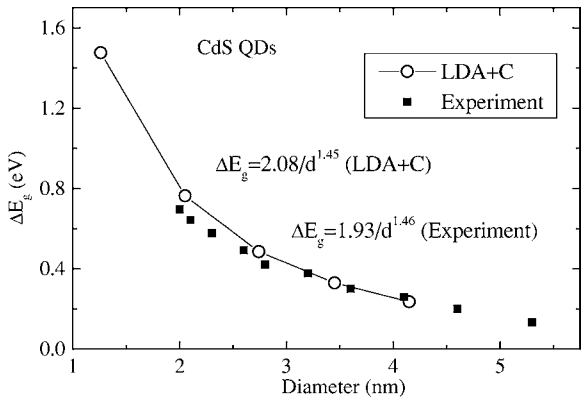

FIG. 14. Size dependence of exciton energies of CdS QDs. Experimental data are from Ref. 83.

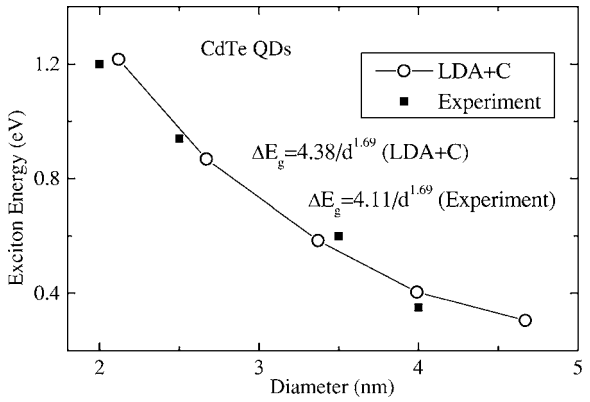

FIG. 15. Size dependence of exciton energies of CdTe QDs. Experimental data are from Ref. 86.

$$\epsilon_{\mathrm{el}}^{-1}(k) = \frac{k^2 + q^2\,\sin(k\rho_\infty)/(\epsilon_\infty^{\mathrm{dot}} k\rho_\infty)}{k^2+q^2}, \tag{6}$$

$$\Delta\epsilon_{\mathrm{ion}}^{-1}(k) = \left(\frac{1}{\epsilon_0^{\mathrm{dot}}} - \frac{1}{\epsilon_\infty^{\mathrm{dot}}}\right)\left(\frac{1/2}{1+\rho_h^2 k^2} + \frac{1/2}{1+\rho_e^2 k^2}\right). \tag{7}$$

Here,

$$\rho_{h,e} = \left(\frac{\hbar}{2m_{h,e}^{*}\omega_{\mathrm{LO}}}\right)^{1/2},$$

ω_{LO} is the longitudinal optical-phonon frequency, and m_e^{*} and m_h^{*} are electron and hole effective masses, respectively. $q = 2\pi^{-1/2}(3\pi^2 n_0)^{1/3}$ is the Thomas-Fermi wave vector (where n_0 is the bulk electron density), and ρ_∞ is the solution of the equation $\sinh(q\rho_\infty)/(q\rho_\infty) = \epsilon_\infty^{\mathrm{dot}}$. The macroscopic high-frequency and low-frequency dielectric constants of the QDs, ϵ_∞ and ϵ_0, are related to the polarizability of the QDs as a whole. The high-frequency dielectric constant is obtained from a modified Penn model where the effective mass band gap is replaced by the *ab initio* charge patch method calculated band gap,

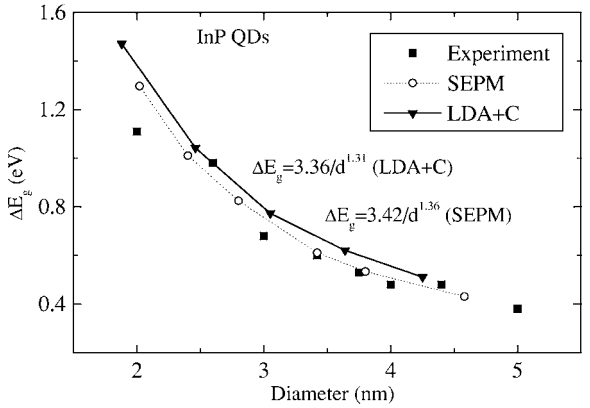

FIG. 16. Comparison of the exciton energy shift (from its bulk value) of InP QDs between experiment, "LDA+C" (present work), and SEPM calculations. Coulomb interactions are considered in this calculations. Experimental data are from Refs. 87 and 88.

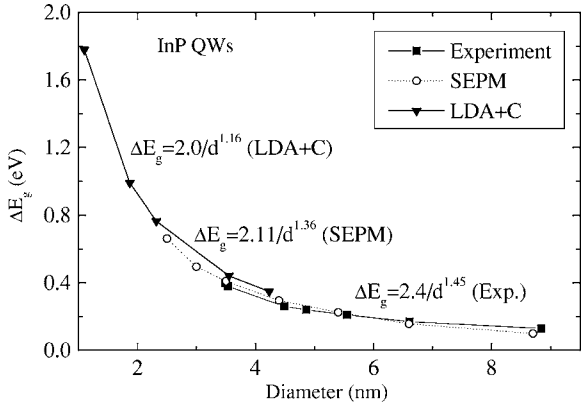

FIG. 17. Comparison of the quantum confinement energy gap of InP QWs between experiment, "LDA+C" (present work), and SEPM calculations. Experimental data are from Refs. 12 and 64.

$$\epsilon_{\infty}^{\mathrm{dot}}(d) = 1 + (\epsilon_{\infty}^{\mathrm{bulk}} - 1)\frac{[E_{\mathrm{gap}}^{\mathrm{bulk}} + \Delta E]}{[E_{\mathrm{gap}}^{\mathrm{dot}} + \Delta E]}, \tag{8}$$

where d is the diameter of QDs; $\epsilon_{\infty}^{\mathrm{bulk}}$ is the bulk high-frequency dielectric constant; $E_{\mathrm{gap}}^{\mathrm{bulk}}+\Delta E$ is the energy of the first pronounced peak in the bulk absorption spectrum; and ΔE can be obtained from bulk by the Penn's model and bulk dielectric constant. The low-frequency dielectric constant is obtained as $\epsilon_0^{\mathrm{dot}}(d)=\epsilon_{\infty}^{\mathrm{dot}}(d)+(\epsilon_0^{\mathrm{bulk}}-\epsilon_{\infty}^{\mathrm{bulk}})$.

III. RESULTS AND DISCUSSIONS

In this section, we will present our calculated results for different semiconductor materials using the approach described in Sec. II. We will compare our results to experimental measurements whenever possible. If the crystal structure is zincblende, then the QW will be in the (111) direction; if the crystal structure is wurtzite, the QW will be in the (0001) direction. For the size dependence of the exciton energy, we will fit our results with a general form of β/d^{α}, where d is the quantum dot or quantum wire diameter.

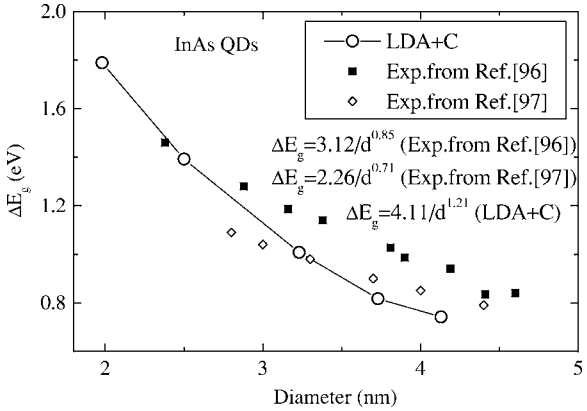

FIG. 18. Size dependence of exciton energies of InAs QDs. Experimental data are from Refs. 96 and 97.

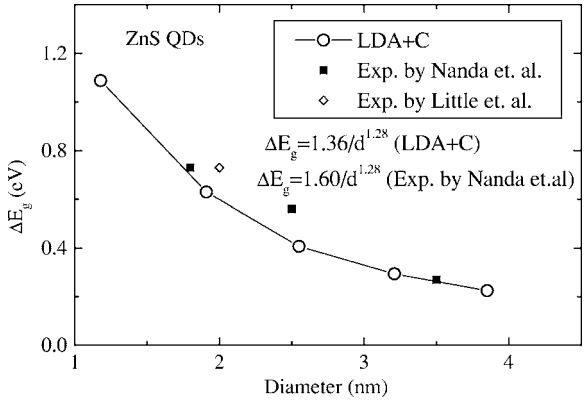

FIG. 19. Size dependence of exciton energies of ZnS QDs. Experimental data are from Refs. 100 and 101.

A. Quantum dots and wires

1. CdSe quantum dots and wires

We assume that CdSe QDs and QWs have a wurtzite crystal structure. The following parameters were used in these calculations: bulk lattice constants a=4.30 Å, c=7.011 Å; $\varepsilon_{\infty}^{\mathrm{bulk}}$=6.2, $\varepsilon_0^{\mathrm{bulk}}$=9.7.[82] For the bulk calculation, we get E_g =0.78 eV and m_e^*=0.069 by "LDA." After the nonlocal pseudopotential fitting (denoted as "LDA+C"), we have E_g =1.56 eV and m_e^*=0.13. The effective-mass by "LDA+C" is in good agreement with experimental data.[82]

We have calculated the wave function charge densities of conduction band minimum (CBM) and valence band maximum (VBM) states for d=1.32 nm and d=4.33 nm QDs (see Fig. 7 and Fig. 8, respectively), and d=1.39 nm and d =4.37 nm QWs (see Fig. 9 and Fig. 10, respectively). First, we see that there is no surface state. This means that the pseudo-hydrogen passivation works very well. We also see that the wave functions in both QD and QW extend all the way to the surfaces. As pointed out in previous studies,[81] the pseudopotential calculated wave functions are less confined than what has been predicted by the simple effective mass model that sets the wave funtion to be zero at the boundary of the dot. In comparison to the QD and the QW CBM states, although they look very different due to different viewing perspectives, the QD CBM and QW CBM have the same atomic characteristics. However, at the VBM state, due to the crystal field splitting, the QD VBM and QW VBM have different polarization.[33] While the QW VBM has z direction polarization, the QD VBM has a predominant xy polarization.

In Fig. 11, we have compared the quantum confinement energy (the energy difference between the nanostructure and the bulk) results between the "LDA+C" and the original "LDA" calculations. We can see that the original LDA cal-

TABLE I. Calculated size-dependence of quantum confinement energies of CdS QWs.

Diameter(nm)	1.33	1.86	2.33	3.48	4.18
ΔE_g (eV)	1.177	0.825	0.586	0.336	0.261

TABLE II. Calculated size-dependence of quantum confinement energies of CdTe QWs.

Diameter(nm)	1.21	2.06	2.56	3.92	4.67
ΔE_g (eV)	1.61	0.857	0.649	0.361	0.28

culation overestimates the quantum confinement effect of the band gap energy by about 0.25 eV in the QDs. While in the CdSe QWs, this overestimation is about 0.18 eV.

The comparison between the experimental[5,6,12,34,65–67] exciton energies and our calculated results (after taking into account the electron-hole Coulomb interactions) are presented in Fig. 12 for CdSe QDs, and in Fig. 13 for CdSe QWs; these two figures also draw comparisons with our previous semiempirical pseudopotential results. All these results agree well with each other. We have fitted our size dependent results as β/d^{α} (d in units of nm and the resulting energy in units of eV). We see that in agreement with previous calculations, the α we got is significantly smaller than the simple effective mass value of 2.

2. CdS quantum dots and wires

We assumed that CdS QDs and QWs have a wurtzite crystal structure. The parameters used in this paper are as follows: bulk lattice constants $a=4.12$ Å, $c=6.73$ Å; $\varepsilon_{\infty}^{\text{bulk}}=5.5$, $\varepsilon_0^{\text{bulk}}=8.7$.[82] For bulk calculation, $E_g=1.315$ eV and $m_e^*=0.127$ by "LDA;" $E_g=2.115$ eV and $m_e^*=0.21$ by "LDA+C."

The comparison with the experimental measurement[43,83–85] for QD are shown in Fig. 14, while the calculated results for QWs are listed in Table I. We see an excellent agreement between theory and experiment. For CdS QD, experimentally there is a large Stokes shift.[43] Previou $k.p$ calculations have shown that this is due to a valence state S-P transition related to spin-orbit coupling. However, since we did not include spin-orbit coupling in our current calculation, such effects cannot be seen in our results. Further study is needed in this regard.

3. CdTe quantum dots and wires

We assumed that CdTe QDs and QWs have a zincblende crystal structure. The parameters used in this paper are as follows: bulk lattice constant $a=6.48$ Å; $\varepsilon_{\infty}^{\text{bulk}}=7.2$, $\varepsilon_0^{\text{bulk}}=10.2$.[82] For bulk calculation, $E_g=0.644$ eV and $m_e^*=0.054$ by "LDA;" $E_g=1.118$ eV and $m_e^*=0.09$ by "LDA+C." Comparisons with the experimental QD results[86,89,90] are shown in Fig. 15, while the calculated QW results are listed in Table II. Experimental work for CdTe QDs is reported in Refs. 86, 89, and 90, and work for CdTe QWs is reported in Refs. 91 and 92.

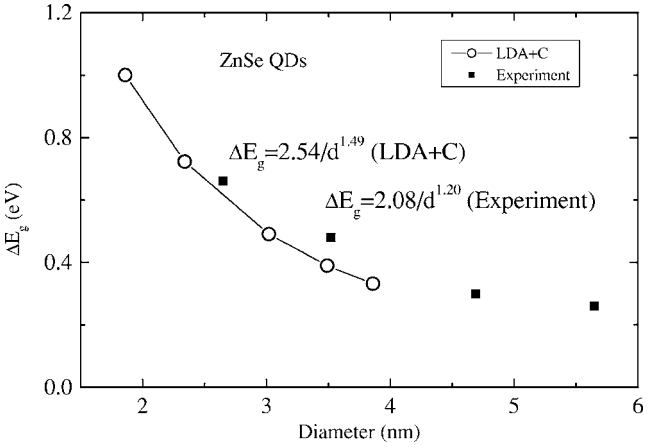

FIG. 20. Size dependence of exciton energies of ZnSe QDs. Experimental data are from Ref. 104.

4. InP quantum dots and wires

We assumed that the InP QDs and QWs have a zinc blende crystal structure. The parameters used in this paper are as following: bulk lattice constants $a=5.87$ Å; $\varepsilon_{\infty}^{\text{bulk}}=10.9$, $\varepsilon_0^{\text{bulk}}=12.5$.[82] For bulk calculation, $E_g=0.543$ eV and $m_e^*=0.045$ by "LDA;" $E_g=1.130$ eV and $m_e^*=0.09$ by "LDA+C," with the effective mass fitted to the experimental data.[82] The calculated InP QD and QW results from LDA+C and the previous SEPM methods are shown in Fig. 16 and Fig. 17, respectively, together with experimental measurements.[64,87,88] We see that, in the QD case, the LDA+C results are slightly higher than the SEPM and experimental values (by about 80 meV).

5. GaAs quantum dots and wires

We assumed that the GaAs QDs and QWs have a zinc blende crystal structure. The parameters used in this paper are as follows: bulk lattice constant $a=5.65$ Å; $\varepsilon_{\infty}^{\text{bulk}}=10.9$, $\varepsilon_0^{\text{bulk}}=12.53$.[82] For bulk calculation, $E_g=0.656$ eV and $m_e^*=0.04$ by "LDA;" $E_g=1.132$ eV and $m_e^*=0.067$ by "LDA+C." The calculated GaAs QDs and QWs results are

TABLE III. Calculated size-dependence of quantum confinement energies of GaAs QDs and QWs. The first line of QDs does not include the Coulomb energies, while the second line of QDs includes the Coulomb energies.

	Diameter(nm)	1.85	2.33	3.01	3.48	3.85
QDs (no)	ΔE_g (eV)	1.849	1.454	1.091	0.961	0.85
QDs	ΔE_g (eV)	1.571	1.253	0.951	0.833	0.738
	Diameter(nm)	1.06	1.80	2.23	3.42	4.08
QWs	ΔE_g (eV)	1.704	1.079	0.901	0.527	0.416

TABLE IV. Calculated size-dependence of quantum confinement energies of InAs QWs.

Diameter(nm)	1.13	1.93	2.39	3.66	4.37
ΔE_g (eV)	2.103	1.221	0.972	0.661	0.504

listed in Table III. Experimental work for GaAs QDs was reported in Refs. 93 and 94; for GaAs QWs, in Refs. 12, 13, and 95.

6. InAs quantum dots and wires

We assumed that the InAs QDs and QWs have a zinc blende crystal structure. The parameters used in this paper are as follows: bulk lattice constant $a=6.06$ Å; $\varepsilon_\infty^{\text{bulk}}=12.25$, $\varepsilon_0^{\text{bulk}}=15.15$.[82] For bulk calculation, $E_g=-0.203$ eV and $m_e^*=0.006$ by "LDA;" $E_g=0.268$ eV and $m_e^*=0.024$ by "LDA+C." The InAs QD results are shown in Fig. 18, together with the experimental measurements.[96,97] We see that while our calculated exciton energies are somewhat smaller than the scanning tunneling microscopy experimental results,[96] especially for large quantum dots, the agreement with the PL measurement[97] is very good. The calculated InAs QW results are listed in Table IV. Experimental work for InAs QDs was reported in Refs. 96–99, while InAs QWs was reported in Refs. 12, 13, and 29.

7. ZnS quantum dots and wires

We assumed that the ZnS QDs and QWs have a wurtzite crystal structure. The parameters used in this paper are as follows: bulk lattice constants $a=3.83$ Å, $c=6.25$ Å; $\varepsilon_\infty^{\text{bulk}}=5.7$, $\varepsilon_0^{\text{bulk}}=9.6$.[82] For bulk calculation, $E_g=1.838$ eV and $m_e^*=0.155$ by "LDA;" $E_g=2.367$ eV and $m_e^*=0.27$ by "LDA+C." The calculated ZnS QD results are shown in Fig. 19, together with experimental data.[100–103] The calculated ZnS QW results are listed in Table V.

8. ZnSe quantum dots and wires

We assumed that the ZnSe QDs and QWs have a zinc blende crystal structure. The parameters used in this paper are as follows: bulk lattice constant $a=5.67$ Å; $\varepsilon_\infty^{\text{bulk}}=5.7$, $\varepsilon_0^{\text{bulk}}=8.6$.[82] For bulk calculation, $E_g=1.092$ eV and $m_e^*=0.083$ by "LDA;" $E_g=1.574$ eV and $m_e^*=0.17$ by "LDA+C." The calculated ZnSe QD results are shown in Fig. 20, together with experimental values.[104–106] The calculated ZnSe QW results are listed in Table VI.

9. ZnTe quantum dots and wires

We assumed that the ZnTe QDs and QWs have a zinc blende crystal structure. The parameters used in this paper

TABLE V. Calculated size-dependence of quantum confinement energies of ZnS QWs.

Diameter(nm)	1.24	1.73	2.16	3.24	3.88
ΔE_g (eV)	0.934	0.712	0.539	0.289	0.215

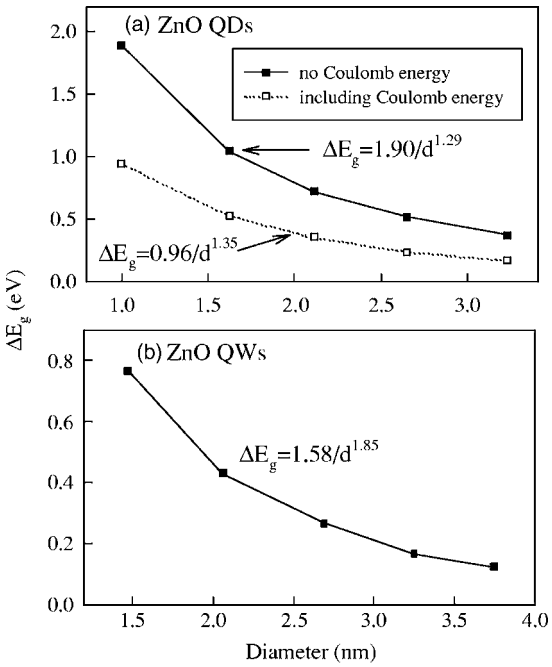

FIG. 21. Size dependence of exciton energies of ZnO QDs (a) and QWs (b).

are as follows: bulk lattice constant $a=6.1$ Å; $\varepsilon_\infty^{\text{bulk}}=7.28$, $\varepsilon_0^{\text{bulk}}=10.3$.[82] For bulk calculation, $E_g=1.092$ eV and $m_e^*=0.083$ by "LDA;" $E_g=1.785$ eV and $m_e^*=0.13$ by "LDA+C." The calculated ZnTe QD and QW results are listed in Table VII.

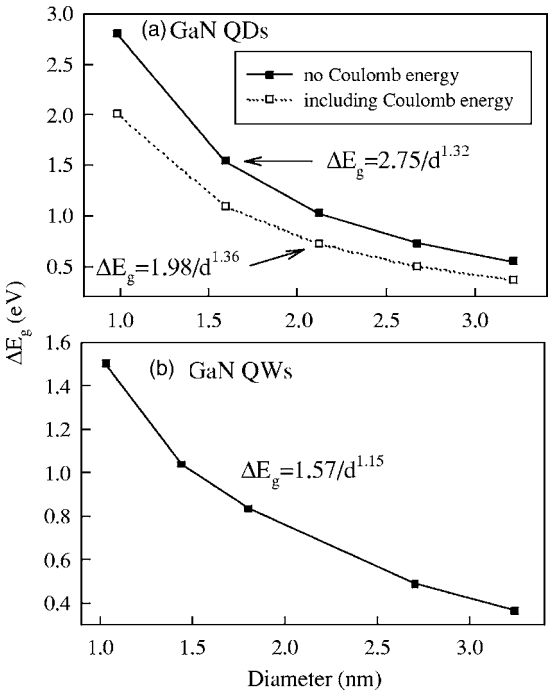

FIG. 22. Size dependence of exciton energies of GaN QDs (a) and QWs (b).

TABLE VI. Calculated size-dependence of quantum confinement energies of ZnSe QWs.

Diameter(nm)	1.06	1.80	2.25	3.43	4.09
ΔE_g (eV)	1.648	0.869	0.647	0.345	0.260

10. ZnO quantum dots and wires

We assumed that the ZnO QDs and QWs have a wurtzite crystal structure. The parameters used in this paper are as follows: bulk lattice constants $a=3.25$ Å, $c=5.31$ Å; $\varepsilon_\infty^{\text{bulk}}=3.7$, $\varepsilon_0^{\text{bulk}}=7.8$.[82] For bulk calculation, $E_g=1.838$ eV and $m_e^*=0.155$ by "LDA;" $E_g=2.367$ eV and $m_e^*=0.27$ by "LDA+C."

The calculated ZnO QD and QW results are shown in Fig. 21(a) and Fig. 21(b), respectively. We see that, for this material, the quantum confinement effect is quite small. At a diameter of 30 Å, the exciton energy increase is only about 200 meV. One reason for this is the relatively large electron effective mass due to the large band gap of this material. In addition, the electron-hole Coulomb interaction has reduced the exciton confinement energy by half as shown in Fig. 21(a). This is due in part to the small dielectric constant $\varepsilon_\infty^{\text{bulk}}$ in this system, which is also related to the large band gap. Thus, in short, a larger band gap binary semiconductor material will have a smaller quantum confinement effect in QD and QW. We find this trend is true across all the materials we studied.

11. GaN quantum dots and wires

We assumed that the GaN QDs and QWs have a wurtzite crystal structure. The parameters used in this paper are as follows: bulk lattice constants $a=3.19$ Å, $c=5.19$ Å; $\varepsilon_\infty^{\text{bulk}}=5.47$, $\varepsilon_0^{\text{bulk}}=10.4$.[82] For bulk calculation, $E_g=2.016$ eV and $m_e^*=0.179$ by "LDA;" $E_g=2.394$ eV and $m_e^*=0.22$ by "LDA+C." The calculated GaN QD and QW results are shown in Fig. 22(a) and Fig. 22(b), respectively.

12. InN quantum dots and wires

We assumed that the InN QDs and QWs have a wurtzite crystal structure. The parameters used in this paper are as follows: bulk lattice constants $a=3.53$ Å, $c=5.76$ Å; $\varepsilon_\infty^{\text{bulk}}=8.4$, $\varepsilon_0^{\text{bulk}}=15.3$.[82,107] For bulk calculation, $E_g=-0.331$ eV and $m_e^*=0.006$ by "LDA;" $E_g=0.597$ eV and $m_e^*=0.084$ by "LDA+C." The calculated InN QD and QW results are shown in Fig. 23(a) and Fig. 23(b), respectively. Experimental work for InN QDs was reported in Ref. 108, while experimental work for InN QWs was reported in Refs. 109 and 110.

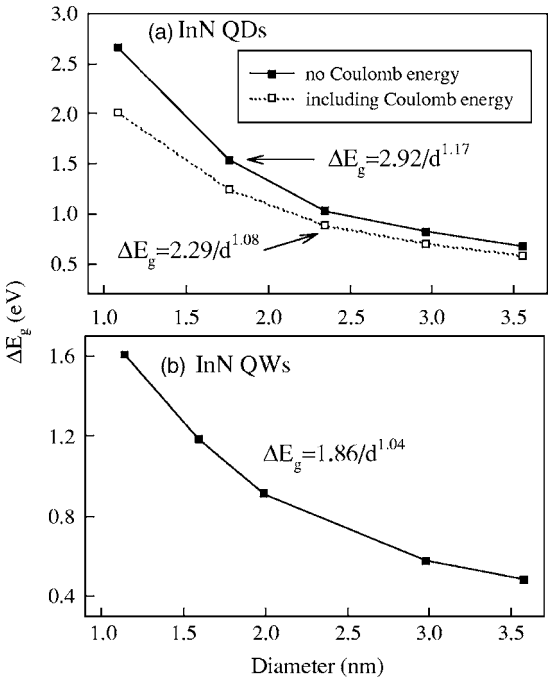

FIG. 23. Size dependence of exciton energies of InN QDs (a) and QWs (b).

13. AlN quantum dots and wires

We assumed that the AlN QDs and QWs have a wurtzite crystal structure. The parameters used in this paper are as follows: bulk lattice constants $a=3.11$ Å, $c=5.08$ Å; $\varepsilon_\infty^{\text{bulk}}=4.68$, $\varepsilon_0^{\text{bulk}}=9.14$.[82] For bulk calculation, $E_g=4.092$ eV and $m_e^*=0.31$ by "LDA;" $E_g=4.45$ eV and $m_e^*=0.34$ by "LDA+C." The calculated AlN QD and QW results are listed in Table VIII. Experimental work for InN QWs was reported in Refs. 111 and 112.

B. Wurtzite vs zinc blende structure

There have been theoretical studies (e.g., see Refs. 113 and 114) comparing the QD and QW electronic structures of wurtzite and zinc blende crystal structures. Here, we have compared the energy gaps (without the electron-hole Cou-

TABLE VII. Calculated size-dependence of quantum confinement energies of ZnTe QDs and QWs. The first line of QDs does not include the Coulomb energies, while the second line of QDs includes the Coulomb energies.

	Diameter(nm)	2.00	2.51	3.25	3.76	4.35
QDs (no)	ΔE_g (eV)	1.454	1.085	0.722	0.604	0.512
QDs	ΔE_g (eV)	1.142	0.836	0.537	0.483	0.406
	Diameter(nm)	1.14	1.94	2.41	3.69	4.40
QWs	ΔE_g (eV)	1.433	0.805	0.616	0.336	0.258

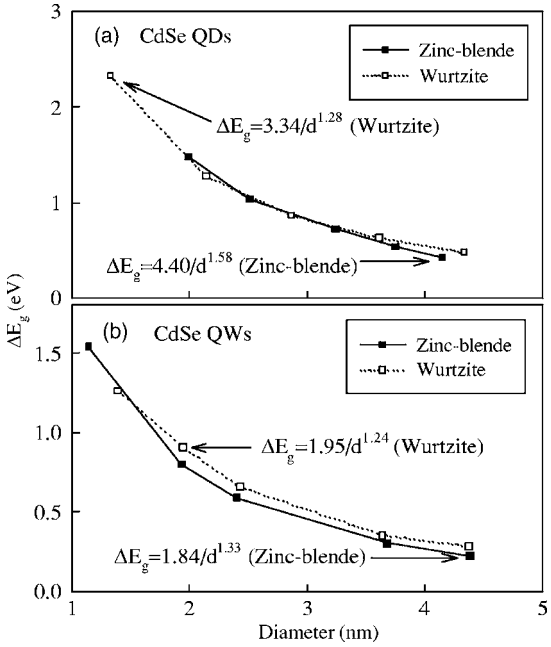

FIG. 24. Size dependence of energy gaps for CdSe QDs (a) and QWs (b). Note, the electron-hole Coulomb interaction is not included, thus (a) is different from Fig. 12.

lomb interaction) of these two different crystal structures for CdSe QDs and QWs. The results are shown in Fig. 24. As we can see, although the wave function symmetry and the fine structures of the energy spectrum might be different, the energy gaps for these two crystal structures are more or less the same.

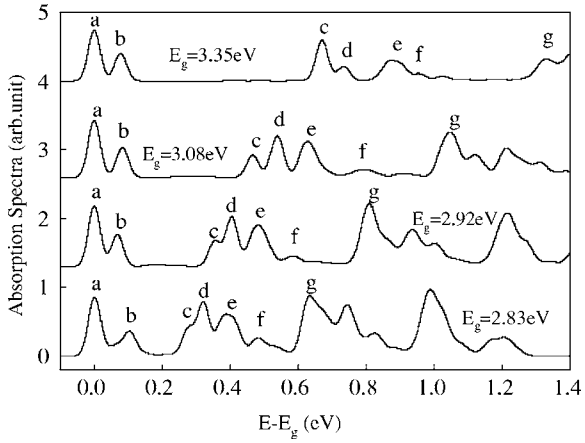

FIG. 25. Theoretical optical absorption spectra of wurtzite structure CdS QDs. Coulomb interaction is taken into account in the calculation. E_g is the ground exciton energy. The four quantum dots from the top curve to the bottom curve are: $Cd_{87}S_{96}$, $Cd_{217}S_{220}$, $Cd_{443}S_{432}$, and $Cd_{750}S_{765}$, respectively. The peak a corresponds to VB1,2,3-CB1 transitions; peak b corresponds to VB7,8,9-CB1 transitions; peak c→ VB1,2,3-CB2,3,4; peak d→ VB4,5-CB2,3,4; peak e→ VB10,11-CB2,3,4; peak g→ VB8,9-CB5,6,7,8,9,10.

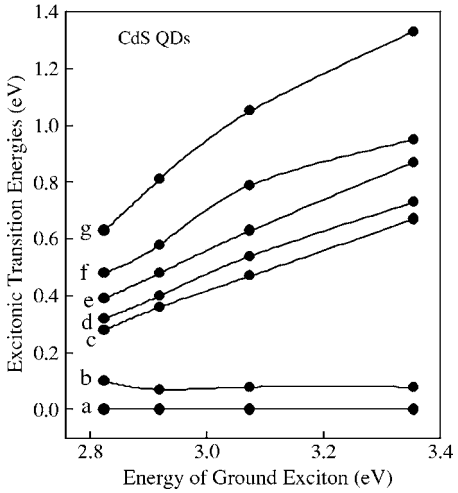

FIG. 26. Theoretical optical absorption peaks of CdS QDs extracted from Fig. 25.

C. Absorption spectra of CdS quantum dots

The optical absorption spectrum intensity is obtained here by summing over the dipole matrix elements coupling hole state (i,v) and electron state (j,c), i.e.,

$$I(E) = \sum_{i,j} \frac{4e^2}{3m^2c^2} |\langle \psi_{i,v}|P_{xyz}|\psi_{j,c}\rangle|^2 f(E - E_{ij}). \quad (9)$$

Here, $f(E-E_{ij})$ is a Gaussian broadening function, and E_{ij} is the energy difference of the valence i and conduction j states including the Coulomb interaction as described in Eq. (4). P_{xyz} is the momentum operator with the subscript "xyz" denoting polarizations.

Figure 25 shows the calculated absorption spectrum (sum over all x,y,z polarizations) for different sized CdS QDs. Following the peak's movement with the size, we have assigned different peaks crossing different QDs. The peaks can be placed into groups: (a, b), (c, d, e, f), (g, etc.). Each group corresponds to one degenerated (or almost degenerated) conduction band state. For example, (a, b) corresponds to the transitions to the first conduction band *s*-like state CB1; (c, d, e, f) correspond to the transitions to the three *p*-like conduction band states CB2,3,4; while (g, etc.) correspond to the transitions to the five *d*-like conduction band states CB5-10.

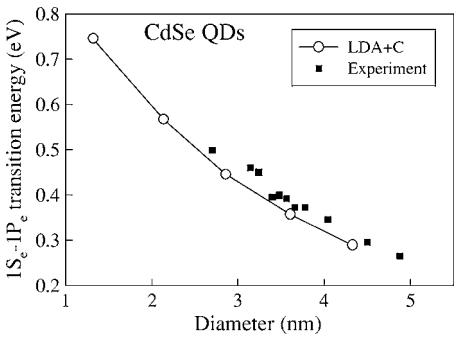

FIG. 27. Size dependence of $1S_e1P_e$ transition energy of *n*-type CdSe QDs.

TABLE VIII. Calculated size-dependence of quantum confinement energies of AlN QDs and QWs. The first line of QDs does not include the Coulomb energies, while the second line of QDs includes the Coulomb energies.

	Diameter(nm)	0.96	1.55	2.07	2.61	3.13
QDs (no)	ΔE_g (eV)	0.982	0.498	0.38	0.284	0.262
QDs	ΔE_g (eV)	0.62	0.26	0.202	0.194	0.186
	Diameter(nm)	1.41	1.76	2.63	3.16	4.01
QWs	ΔE_g (eV)	0.61	0.455	0.305	0.247	0.185

Each peak within one group corresponds to the transition from different valence band states (or degenerated valence band states). For example, peak *a* corresponds to the transition from VB1,2,3 to CB1, while *b* corresponds to the VB7,8,9 to CB1 transition. More assignments are given in the caption of Fig. 25. The peak energies of Fig. 25 are plotted as functions of the lowest exciton energy in Fig. 26. We see that although the energy distances between different groups increase significantly when the size of the dot decreases, the distances between the peaks within a group stay almost the same. This is because the confinement effects for the valence bands are small. Besides, the electron-hole Coulomb interaction also plays a part in determining the absorption spectrum peak positions. Our calculated absorption spectrum invites experimental verification.

D. Comparison of quantum confinement effects between quantum wires and dots

In a previous study,[62] we have investigated the ratio of quantum confinements between QDs and QWs with the same diameter for the same semiconductor materials. However, in that study, the bulk LDA band structure (e.g., the effective mass) is not corrected. Here, we have reinvestigated this issue using the "LDA+C" results. In order to yield a constant ratio between QW and QD confinements for different sizes d, we first need to fit QW and QD results with the same $1/d^{\alpha}$ scaling. In the fitting reported above, the exponents α for QDs and QWs are often slightly different. Here, we have refitted all of our QD and QW results with the same exponent for a given semiconductor material without Coulomb energy. The resulting ratio between the QWs and QDs for all the materials we have studied are listed in Table IX. We see that the majority of them are close to the simple effective mass result of 0.586, with a few exceptions. For AlN, this ratio is 0.971, which means that the QW confinement is almost as large as the QD confinement. Similarly the ratio for InN is also quite big: 0.676. On the other hand, the ratio for CdTe and ZnTe are significantly smaller than the effective mass result. Interestingly, from the systems we have investigated, it appears that this ratio depends more sensitively on the anion rather than the cation.

E. $1S_e$-$1P_e$ transition energy of CdSe quantum dots

A colloidal quantum dot is much more difficult to be doped as *n*-type material, compared to its bulk counterpart.[76–78] However, in Ref. 76, CdSe semiconductor nanocrystals have been successfully doped as *n*-type material, with electrons in quantum confined states. The *n*-type doped QD provides an opportunity to conduct infrared absorption between the conduction band S state ($1S_e$) to conduction band P state ($1P_e$).[76] This experimental $1S_e$-$1P_e$ transition energy is compared with our calculated results for CdSe QD in Fig. 27. The agreement is excellent.

IV. CONCLUSIONS

In this work, we have performed *ab initio* calculations to study the surface-passivated thousand atom semiconductor quantum dots and wires. We have systematically calculated the electronic states of group III-V (GaAs, InAs, InP, GaN, AlN, and InN) and group II-VI (CdSe, CdS, CdTe, ZnSe, ZnS, ZnTe, and ZnO) quantum dots and wires. The LDA bulk band structure has been corrected to yield the experimental effective mass by modifying the nonlocal pseudopotentials. We have calculated exciton energies of quantum dots including the screened Coulomb interactions. We have found the following results: (1) In most cases, our calculated exciton energies agree well with the experimental photoluminescence results. When there are no good experimental measurements at the present (especially for quantum wires), our calculated results can be used as predictions and benchmarks. (2) For CdSe and InP quantum dots, wires, and InAs dots that have been studied previously using the semiempirical pseudopotential method (SEPM) or the EPM method,

TABLE IX. The ratios between the QWs quantum confinement and QDs quantum confinement for different semiconductor materials.

III–V	GaAs	InAs	InP	GaN	AlN	InN	
QW/QD	0.532	0.546	0.538	0.597	0.971	0.676	
II–VI	CdSe	CdS	CdTe	ZnSe	ZnS	ZnTe	ZnO
QW/QD	0.596	0.589	0.495	0.561	0.598	0.512	0.599

our current results agree well with the previous results. This is an indication of the reliability and consistency of both methods, but the current method provides a flexibility to study any given semiconductor materials. (3) The ratios of band-gap-increases between quantum wires and dots have been investigated. Although there is a material dependence, the majority of them are close to the simple effective mass ratio of 0.586. One major exception is AlN, which has a large ratio of 0.97. (4) The size-dependence of $1S_e$-$1P_e$ transition energies of CdSe quantum dots with a wurtzite structure agrees well with the experimental measurement, and (5) the calculated higher excited state energies for CdS quantum dots are presented. (6) For wurtzite and zincblende CdSe, we find very small differences in band gap energies for both QDs and QWs.

ACKNOWLEDGMENTS

The authors would like to thank Professor A. P. Alivisatos, Professor L. E. Brus, Professor W. E. Buhro, Professor Peidong Yang, Dr. Yi Cui, and Dr. Su-Huai Wei for helpful discussions. This work was supported by U.S. Department of Energy under Contract No. DE-AC03-76SF00098. This research used the resources of the National Energy Research Scientific Computing Center.

*Electronic address: lwwang@lbl.gov

[1] A. P. Alivisatos, Science **271**, 933 (1996).
[2] A. P. Alivisatos, J. Phys. Chem. **100**, 13226 (1996).
[3] L. E. Brus, J. Chem. Phys. **80**, 4403 (1984).
[4] U. Woggon, *Optical Properties of Semiconductor Quantum Dots* (Springer-Verlag, Berlin, 1996).
[5] C. B. Murray, D. J. Norris, and M. G. Bawendi, J. Am. Chem. Soc. **115**, 8706 (1993).
[6] A. I. Ekimov, F. Hache, M. C. Schanne-Klein, D. Ricard, C. Flytzanis, I. A. Kudryavtsev, T. V. Yazeva, A. V. Rodina, and Al. L. Efros, J. Opt. Soc. Am. B **10**, 100 (1993).
[7] G. A. Ozin, Adv. Mater. (Weinheim, Ger.) **4**, 612 (1992).
[8] A. D. Yoffe, Adv. Phys. **42**, 173 (1993).
[9] A. D. Yoffe, Adv. Phys. **50**, 1 (2001).
[10] M. Law, J. Goldberger, and P. Yang, Annu. Rev. Mater. Res. **34**, 83 (2004).
[11] Y. N. Xia, P. Yang, Y. Sun, Y. Wu, B. Mayers, B. Gates, Y. Yin, F. Kim, and H. Yan, Adv. Mater. (Weinheim, Ger.) **15**, 353 (2003).
[12] X. Duan, C. M. Lieber, Adv. Mater. (Weinheim, Ger.) **12**, 298 (2000).
[13] T. J. Trentler, K. M. Hickman, S. C. Goel, A. M. Viano, P. C. Gibbons, and W. E. Buhro, Science **270**, 1791 (1995).
[14] M. Kazes, D. Y. Lewis, Y. Ebenstein, T. Mokari, and U. Banin, Adv. Mater. (Weinheim, Ger.) **14**, 317 (2002).
[15] V. I. Ekimov, A. A. Mikhailovsky, S. Xu, A. Malko, J. A. Hollingsworth, C. A. Leatherdale, H. J. Eisler, and M. G. Bawendi, Science **290**, 314 (2000).
[16] M. Achermann, M. A. Petruska, S. Kos, D. L. Smith, D. D. Koleske, and V. I. Ekimov, Nature (London) **429**, 642 (2004).
[17] W. U. Huynh, J. J. Dittmer, and A. P. Alivisatos, Science **295**, 2425 (2002).
[18] D. L. Klein, R. Roth, A. K. L. Lim, A. P. Alivisatos, and P. L. McEuen, Nature (London) **389**, 699 (1997).
[19] A. P. Alivisatos, Nat. Biotechnol. **22**, 47 (2004).
[20] M. Bruchez, M. Moronne, P. Gin, S. Weiss, and A. P. Alivisatos, Science **281**, 2013 (1998).
[21] W. C. W. Chan and S. Nie, Science **281**, 2016 (1998).
[22] Y. Cui, Q. Wei, H. Park, and C. M. Lieber, Science **293**, 1289 (2001).
[23] X. Gao, Y. Cui, R. M. Levenson, L. W. K. Chung, and S. Nie, Nat. Biotechnol. **22**, 969 (2004).
[24] J. Li and L. W. Wang, Nano Lett. **3**, 1357 (2003).
[25] X. Peng, L. Manna, W. D. Yang, J. Wickham, E. Scher, A. Kadavanich, and A. P. Alivisatos, Nature (London) **404**, 59 (2000).
[26] L. Manna, E. Scher, and A. P. Alivisatos, J. Am. Chem. Soc. **122**, 12700 (2000).
[27] L. Manna, D. Milliron, A. Meisel, E. Scher, and A. P. Alivisatos, Nat. Mater. **2**, 382 (2003).
[28] W. E. Buhro and V. L. Colvin, Nat. Mater. **2**, 138 (2003).
[29] S. H. Kan, T. Mokari, E. Rothenberg, and U. Bannin, Nat. Mater. **2**, 155 (2003).
[30] H. Yan, R. He, J. Pham, and P. Yang, Adv. Mater. (Weinheim, Ger.) **15**, 402 (2003).
[31] J. Hu, Y. Zhang, B. Liu, J. Liu, H. Zhou, Y. Xu, Y. Jiang, Z. Yang, and Z. Q. Tian, J. Am. Chem. Soc. **126**, 9470 (2004).
[32] J. Hu, L. Li, W. Yang, L. Manna, L. W. Wang, and A. P. Alivisatos, Science **292**, 2060 (2001).
[33] J. Hu, L. W. Wang, L. Li, W. Yang, and A. P. Alivisatos, J. Phys. Chem. B **106**, 2447 (2002).
[34] Al. L. Efros, M. Rosen, M. Kuno, M. Nirmal, D. J. Norris, and M. Bawendi, Phys. Rev. B **54**, 4843 (1996).
[35] J. B. Xia, Phys. Rev. B **40**, 8500 (1989).
[36] J. B. Xia and J. Li, Phys. Rev. B **60**, 11540 (1999).
[37] L. W. Wang and A. Zunger, Phys. Rev. B **54**, 11417 (1996).
[38] S. S. Li, J. B. Xia, Z. L. Yuan, Z. Y. Xu, W. Ge, X. R. Wang, Y. Wang, J. Wang, and L. L. Chang, Phys. Rev. B **54**, 11575 (1996).
[39] S. S. Li and J. B. Xia, Phys. Rev. B **55**, 15434 (1997).
[40] S. J. Prado, C. Trallero-Giner, A. M. Alcalde, V. Lopez-Richard, and G. E. Marques, Phys. Rev. B **68**, 235327 (2003).
[41] V. A. Fonoberov, E. P. Pokatilov, and A. A. Balandin, Phys. Rev. B **66**, 085310 (2002).
[42] M. Nirmal, D. J. Norris, M. Kuno, M. G. Bawendi, Al. L. Efros, and M. Rosen, Phys. Rev. Lett. **75**, 3728 (1995).
[43] Z. Yu, J. Li, D. B. Connor, L. W. Wang, and P. F. Barbara, J. Phys. Chem. B **107**, 5670 (2003).
[44] N. A. Hill and K. B. Whaley, Phys. Rev. Lett. **75**, 1130 (1995).
[45] J. Perez-Conde and A. K. Bhattacharjee, Phys. Rev. B **63**, 245318 (2001).
[46] G. Allan, Y. M. Niquet, and C. Delerue, Appl. Phys. Lett. **77**, 639 (2000).
[47] J. G. Diaz, J. Planelles, G. W. Bryant, and J. Aizpurua, J. Phys. Chem. B **108**, 17800 (2004).
[48] J. G. Diaz and J. Planelles, Langmuir **20**, 11278 (2004).

[49] G. W. Bryant and W. Jaskolski, Phys. Rev. B **67**, 205320 (2003).
[50] L. W. Wang and A. Zunger, J. Chem. Phys. **100**, 2394 (1994).
[51] L. W. Wang and A. Zunger, Phys. Rev. Lett. **73**, 1039 (1994).
[52] L. W. Wang and A. Zunger, J. Phys. Chem. **98**, 2158 (1994).
[53] L. W. Wang and A. Zunger, Phys. Rev. B **53**, 9579 (1996).
[54] L. W. Wang, A. Franceschetti, and A. Zunger, Phys. Rev. Lett. **78**, 2819 (1997).
[55] H. Fu, L. W. Wang, and A. Zunger, Appl. Phys. Lett. **71**, 3433 (1997).
[56] L. W. Wang, M. Califano, A. Zunger, and A. Franceschetti, Phys. Rev. Lett. **91**, 056404 (2003).
[57] J. Li and L. W. Wang, Nano Lett. **4**, 29 (2004).
[58] D. Milliron, S. M. Hughes, Y. Cui, L. Manna, J. Li, L. W. Wang, and A. P. Alivisatos, Nature (London) **430**, 190 (2004).
[59] J. Li and L. W. Wang, Appl. Phys. Lett. **84**, 3648 (2004).
[60] J. Li and L. W. Wang, Appl. Phys. Lett. **85**, 2929 (2004).
[61] H. Jiang, H. U. Baranger, and W. Yang, Phys. Rev. B **68**, 165337 (2003).
[62] J. Li and L. W. Wang, Chem. Mater. **16**, 4012 (2004).
[63] L. W. Wang and J. Li, Phys. Rev. B **69**, 153302 (2004).
[64] H. Yu, J. Li, R. A. Loomis, L. W. Wang, and W. E. Buhro, Nat. Mater. **2**, 517 (2003).
[65] H. Yu, J. Li, R. A. Loomis, P. C. Gibbons, L. W. Wang, and W. E. Buhro, J. Am. Chem. Soc. **125**, 16168 (2003).
[66] D. J. Norris, A. Sacra, C. B. Murray, and M. G. Bawendi, Phys. Rev. Lett. **72**, 2612 (1994).
[67] D. J. Norris and M. G. Bawendi, Phys. Rev. B **53**, 16338 (1996).
[68] D. Katz, T. Wizansky, O. Millo, E. Rothenberg, T. Mokari, and U. Banin, Phys. Rev. Lett. **89**, 086801 (2002).
[69] N. LeThomas, E. Herz, O. Schops, and U. Woggon, Phys. Rev. Lett. **94**, 016803 (2005).
[70] L. W. Wang and A. Zunger, J. Phys. Chem. B **102**, 6449 (1998).
[71] J. Li and L. W. Wang, Nano Lett. **3**, 101 (2003).
[72] H. Fu and A. Zunger, Phys. Rev. B **57**, R15064 (1998).
[73] J. Li and J. B. Xia, Phys. Rev. B **61**, 15880 (2000).
[74] J. Li and J. B. Xia, Phys. Rev. B **62**, 12613 (2000).
[75] W. H. Zheng, J. B. Xia, and K. W. Cheah, J. Phys.: Condens. Matter **9**, 5105 (1997).
[76] M. Shim and P. Guyot-Sionnest, Nature (London) **407**, 981 (2000).
[77] M. Shim, C. J. Wang, and P. Guyot-Sionnest, J. Phys. Chem. B **105**, 2369 (2001).
[78] D. Yu, C. Y. Wang, and P. Guyot-Sionnest, Science **300**, 1277 (2003).
[79] http://hpcrd. lbl.gov/linwang/PEtot/PEtot.html.
[80] L. W. Wang, Phys. Rev. Lett. **88**, 256402 (2002).
[81] A. Franceschetti and A. Zunger, Phys. Rev. Lett. **78**, 915 (1997).
[82] *Semiconductors: Data Handbook*, 3rd ed., edited by O. Madelung (Springer-Verlag, Berlin, 2004).
[83] W. W. Yu and X. Peng, Angew. Chem., Int. Ed. **41**, 2368 (2002).
[84] Y. Wang and N. Herron, Phys. Rev. B **42**, 7253 (1990).
[85] T. Vossmeyer, L. Katsikas, M. Giersig, I. G. Popovic, K. Diesner, A. Chemseddine, A. Eychmuller, and H. Weller, J. Phys. Chem. **98**, 7665 (1994).
[86] T. Rajh, O. I. Micic, and A. J. Nozic, J. Phys. Chem. **97**, 11999 (1993).
[87] O. I. Micic, C. J. Curtis, K. M. Jones, J. R. Sprague, and A. J. Nozik, J. Phys. Chem. **98**, 4966 (1994).
[88] A. A. Guzelian, J. E. B. Katari, A. V. Kadavanich, U. Banin, K. Hamad, E. Juban, A. P. Alivisatos, R. H. Wolters, C. C. Arnold, and J. R. Health, J. Phys. Chem. **100**, 7212 (1996).
[89] Y. Masumoto and K. Sonobe, Phys. Rev. B **56**, 9734 (1997).
[90] Y. Mastai and G. Hodes, J. Phys. Chem. B **101**, 2685 (1997).
[91] Z. Tang, N. A. Kotov, and M. Giersig, Science **297**, 237 (2002).
[92] J. Lee, A. O. Govorov, J. Dulka, and N. A. Kotov, Nano Lett. **4**, 2323 (2004).
[93] H. Uchida, C. J. Curtis, P. V. Kamat, K. M. Jones, and A. J. Nozik, J. Phys. Chem. **96**, 1156 (1992).
[94] O. V. Salata, P. J. Dobson, P. J. Hull, and J. I. Hutchison, Appl. Phys. Lett. **65**, 189 (1994).
[95] H. Yu and W. E. Buhro, Adv. Mater. (Weinheim, Ger.) **15**, 416 (2003).
[96] U. Banin, Y. W. Cao, D. Katz, and O. Millo, Nature (London) **400**, 542 (1999).
[97] U. Banin *et al.*, J. Chem. Phys. **109**, 2306 (1998).
[98] D. Katz, O. Millo, S. H. Kan, and U. Banin, Appl. Phys. Lett. **79**, 117 (2001).
[99] A. A. Guzelian, U. Banin, A. V. Kadavanich, X. Peng, and A. P. Alivisatos, Appl. Phys. Lett. **69**, 1432 (1996).
[100] J. Nanda, S. Sapra, and D. D. Sarma, Chem. Mater. **12**, 1018 (2000).
[101] R. B. Little, M. A. El-Sayed, G. W. Bryant, and S. Burke, J. Chem. Phys. **114**, 1813 (2001).
[102] H. Zhang, B. Gilbert, F. Huang, and J. F. Banfield, Nature (London) **424**, 1025 (2003).
[103] H. Zhang and J. F. Banfield, Nano Lett. **4**, 713 (2004).
[104] C. A. Smith, H. W. H. Lee, V. J. Leppert, and S. H. Risbud, Appl. Phys. Lett. **75**, 1688 (1999).
[105] M. A. Hines and P. Guyot-Sionnest, J. Phys. Chem. B **102**, 3655 (1998).
[106] N. Chestnoy, R. Hull, and L. E. Brus, J. Chem. Phys. **85**, 2237 (1986).
[107] A. G. Bhuiyan, A. Hashimoto, and A. Yamamoto, J. Appl. Phys. **94**, 2779 (2003).
[108] O. Briot, B. Maleyre, and S. Ruffenach, Appl. Phys. Lett. **83**, 2919 (2003).
[109] J. Zhang, L. Zhang, X. Peng, and X. Wang, J. Mater. Chem. **12**, 802 (2002).
[110] J. Xiao, Y. Xie, and W. Luo, Inorg. Chem. **42**, 107 (2003).
[111] J. Liu, X. Zhang, Y. J. Zhang, R. R. He, and J. Zhu, J. Mater. Res. **16**, 3133 (2001).
[112] C. Xu, L. Xue, C. Yin, and G. Wang, Phys. Status Solidi A **198**, 329 (2003).
[113] H. H. von Grunberg, Phys. Rev. B **55**, 2293 (1997).
[114] A. Bagga, P. K. Chattopadhyay, and S. Ghosh, Phys. Rev. B **68**, 155331 (2003).